JOURNAL OF Materials CHEMISTRY

A new anionic conductive vitreous phase based on bismuth, lead, cadmium, oxygen and fluorine: electrical properties and structural study of the recrystallized phase

Françoise Désanglois,[a] Claudine Follet-Houttemane*[a] and Jean-Claude Boivin[b]

[a]*Laboratoire de Cristallochimie et Physicochimie du Solide, UPRESA 8012, ENSCL, BP 108, 59652 Villeneuve d'Ascq cedex, France*
[b]*Laboratoire de Matériaux Avancés Céramiques, UPRES EA 2443, ISTV, UVHC, BP 311, 59304 Valenciennes cedex, France. E-mail: claudine.follet@univ-valenciennes.fr*

Received 28th February 2000, Accepted 12th March 2000
Published on the Web 17th May 2000

Investigations in the Bi_2O_3–CdO–PbF_2 system using silica tubes as synthesis containers indicate the existence of a large vitreous domain. Structural determination, using powder diffraction and Rietveld methods, has shown that the recrystallized phase is isotypic to the trigonal phase belonging to the Bi_2O_3–PbO–PbF_2 system. Raman studies evidence boson and large peaks, typical of a vitreous phase containing lead in its formulation. Conductivity measurements display σ values close to 10^{-3} S cm^{-1} at 250 °C with an activation energy of 0.6 eV. These values are among the best obtained for an anionic conductive glass.

Oxide and fluoride solid electrolytes are attractive materials for developing new devices, such as solid oxide fuel cells, gas sensors or solid state batteries. Many research studies are still in progress on these materials, but there has been rather limited interest in oxyfluoride electrolytes. However, from our point of view, they offer a real opportunity to develop interesting new materials, which, quite often, are more stable and easier to synthesize than many fluoride phases and exhibit high conductivity at moderate temperatures.[1–4]

For several years, we have investigated bismuth based oxyfluorides. Previous results have been reported on phases belonging to the Bi_2O_3–CdO–PbF_2 system.[5] Syntheses performed in sealed gold tubes have allowed the identification of two crystallized solid solutions (I and H) and a vitreous domain (G) (Fig. 1). Conductivity measurements showed that, of these phases, the vitreous phase exhibits the highest ionic conductivity. However, the σ values were shown to be strongly dependent upon the composition of the glass, particularly on the O/F ratio. The present paper deals with the results of recent investigations using new synthesis conditions in order to obtain the glass over a larger range of compositions.

Experimental

High purity Bi_2O_3 and CdO from Aldrich, and PbF_2 from Alfa were used as starting materials. Bi_2O_3 was first heated for several hours at 600 °C to eliminate any traces of carbonates and hydroxides.

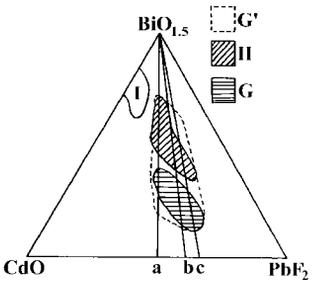

Fig. 1 Solid solutions (I and H) and vitreous (G) domains (sealed gold tubes) and vitreous (G′) domain (silica tubes) in the Bi_2O_3–CdO–PbF_2 system.

The experimental procedure was that described by Govinda Rao *et al.*[6] Appropriately weighed quantities of Bi_2O_3, CdO and PbF_2 were mixed and melted in short, unsealed, quartz tubes using an oxyacetylene flame until a uniformly clear melt was obtained. The melt was kept at 700–750 °C for one or two minutes, then poured on a platinum plate. In order to obtain a glass, these materials need to be quickly quenched.

The formation of a vitreous phase was controlled by DSC measurements and X-ray powder diffraction using a Guinier de Wolff camera. The glass stability in air and the nature of the phase obtained during recrystallization from different glass compositions were examined using a high temperature X-ray diffraction Guinier–Lenné camera.

The compositions of the glasses (ratio of fluorine, introduction of silica from containers into the samples) were controlled by titration, TGA measurements and IR spectroscopy.

An RT 30 Dilor spectrometer with a Kr^+ or Ar^+ Spectra Physics model 2020 laser was used for Raman spectroscopy experiments.

Conductivity measurements were performed on pellets using a Solartron 1174 frequency response analyzer in the range of 1–10^6 Hz. Gold electrodes were deposited by sputtering on opposite plate faces of each sample before analysis.

Results and discussion

Vitreous phase limits and characteristic temperatures

Fig. 1 summarizes the I, H and G phases obtained by synthesis in gold sealed tubes. In a previous study,[5] the gold tubes were heated at 750 °C for 15 minutes in a horizontal furnace, then quenched into water. On the same figure, the limits of the vitreous domain noted G′ have been added. The lines denoted a, b, and c represent three pseudo-binary lines. Along these lines, the formulation of the compounds may be denoted as:

$$\text{line a}: Bi_{2-2x}Cd_xPb_xO_{3-2x}F_{2x}$$

$$\text{line b}: Bi_{2-2x}Cd_{0.8x}Pb_{1.2x}O_{3-2.2x}F_{2.4x}$$

$$\text{line c}: Bi_{2-2x}Cd_{0.7x}Pb_{1.3x}O_{3-2.3x}F_{2.6x}$$

To determine the domain limits, numerous other pseudo-binary lines were explored.

DOI: 10.1039/b002038i

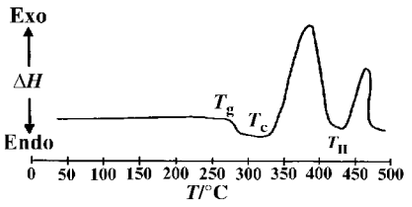

Fig. 2 DSC for $Bi_{0.8}Cd_{0.6}Pb_{0.6}O_{1.8}F_{1.2}$.

A comparison between the two synthesis methods shows a considerable extent of the vitreous phase toward pure Bi_2O_3, when using quartz tubes. This is due to a more efficient quenching rate. No trace of crystallized phase (H phase) was identified for all samples belonging to this domain.

Fig. 2 represents the DSC curve obtained for the $Bi_{0.8}Cd_{0.6}Pb_{0.6}O_{1.8}F_{1.2}$ compound (pseudo-binary a, with $x=0.6$). A small decrease of the base line is observed at 280 °C which can be assigned to T_g. The strong exothermic peak at 340 °C is associated with the recrystallization of the glass (T_c). The third peak (T_H) corresponds to the decomposition of the crystalline phase and is accompanied by a fluorine loss which is clearly evidenced by thermogravimetric analysis.

Table 1 reports the characteristic temperatures for several compositions belonging to the different lines investigated in the ternary diagram. The corresponding O/F ratio is also reported.

High temperature X-ray diffraction patterns showed that the recrystallized phase is isotypic to the H phase identified when using the gold tube synthesis route.[5] There is only one type of recrystallized phase for all the glasses belonging to the G′ domain.

Composition

The synthesis in quartz tubes was carried out in air. We studied the fluorine content and investigated whether silica from the quartz tube reacted with the glass sample.

The fluorine ratio was determined by titration, with a specific electrode, against thorium nitrate. For each G′ sample analyzed, several previous titrations were made: the first against a solution of NaF or PbF_2 with a concentration of F^- similar to the G′ sample content; and another titration, when the G and G′ domains were in agreement, with a solution of the G sample having the same starting composition. The concentrations determined by titration for G′ were always as expected in comparison with the starting compositions.

The fluorine content was also studied by thermogravimetric analysis. Fig. 3 shows the curve obtained for $Bi_{0.8}Cd_{0.6}Pb_{0.6}O_{1.8}F_{1.2}$ (pseudo-binary a, with $x=0.6$). The theoretical

Table 1 F/O ratio, T_g, T_c and T_H for several samples belonging to a, b or c pseudo-binary lines. Pseudo-binary a: $Bi_{2-2x}Cd_xPb_xO_{3-2x}F_{2x}$. Pseudo-binary b: $Bi_{2-2x}Cd_{0.8x}Pb_{1.2x}O_{3-2.2x}F_{2.4x}$. Pseudo-binary c: $Bi_{2-2x}Cd_{0.7x}Pb_{1.3x}O_{3-2.3x}F_{2.6x}$

Composition (pseudo-binary line)	F/O	T_g/°C	T_c/°C	T_H/°C
$Bi_{1.48}Cd_{0.26}Pb_{0.26}O_{2.48}F_{0.52}$ (a)	0.210	316	420	490
$Bi_{1.28}Cd_{0.36}Pb_{0.36}O_{2.28}F_{0.72}$ (a)	0.316	310	410	470
$Bi_{1.2}Cd_{0.4}Pb_{0.4}O_{2.2}F_{0.8}$ (a)	0.364	298	380	450
$Bi_{1.2}Cd_{0.32}Pb_{0.48}O_{2.12}F_{0.96}$ (b)	0.453	293	369	437
$Bi_{1.2}Cd_{0.28}Pb_{0.52}O_{2.08}F_{1.04}$ (c)	0.500	288	361	426
$BiCd_{0.5}Pb_{0.5}O_2F$ (a)	0.500	290	363	428
$BiCd_{0.4}Pb_{0.6}O_{1.9}F_{1.2}$ (b)	0.632	284	350	412
$Bi_{0.8}Cd_{0.6}Pb_{0.6}O_{1.8}F_{1.2}$ (a)	0.667	281	343	408
$Bi_{0.8}Cd_{0.48}Pb_{0.72}O_{1.68}F_{1.44}$ (b)	0.857	267	335	400
$Bi_{0.6}Cd_{0.7}Pb_{0.7}O_{1.6}F_{1.4}$ (a)	0.875	272	340	400
$Bi_{0.8}Cd_{0.42}Pb_{0.78}O_{1.62}F_{1.56}$ (c)	0.963	261	332	398
$Bi_{0.4}Cd_{0.8}Pb_{0.8}O_{1.4}F_{1.6}$ (a)	1.143	252	330	395
$Bi_{0.6}Cd_{0.56}Pb_{0.84}O_{1.46}F_{1.68}$ (b)	1.151	250	325	395
$Bi_{0.6}Cd_{0.49}Pb_{0.91}O_{1.39}F_{1.82}$ (c)	1.309	225	275	388
$Bi_{0.4}Cd_{0.64}Pb_{0.96}O_{1.24}F_{1.92}$ (b)	1.548	217	268	385
$Bi_{0.4}Cd_{0.56}Pb_{1.04}O_{1.16}F_{2.08}$ (c)	1.793	215	267	384

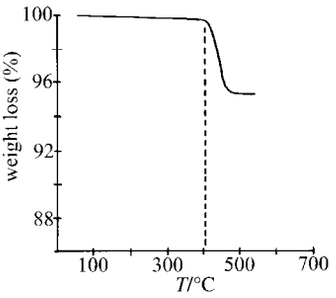

Fig. 3 TGA for $Bi_{0.8}Cd_{0.6}Pb_{0.6}O_{1.8}F_{1.2}$.

fluorine weight loss percentage, calculated from the starting composition, is 4%, assuming that part of the lost fluorine is substituted by oxide ions. At about 400 °C, a weight loss is observed: a peak was also observed at this temperature by DSC and was attributed to a fluorine loss. The experimental weight loss percentage corresponds to the theoretical value. These thermal analysis results show that there is no loss of fluorine during the synthesis. This can be explain by the rapidity of the heating during the synthesis. The heating rate must be higher than the kinetics of fluorine loss.

We also investigated whether silica from the containers was introduced into our glass samples. Fig. 4a shows the infra-red spectrum of the $Bi_{0.8}Cd_{0.6}Pb_{0.6}O_{1.8}F_{1.2}$ compound (pseudo-binary a, with $x=0.6$). Fig. 4b shows the spectrum of a silica tube. No peak typical of silica appears in the IR spectrum of our glass sample. Therefore the quartz synthesis tubes do not interfere in the synthesis.

Raman spectroscopy results

Raman spectra were recorded from samples belonging to both the H and G phases synthesized in gold tubes and to the G′ phase synthesized in silica tubes.

The Raman diffusion spectra of the H and G samples are presented in Fig. 5. The results are those of the pseudo-binary a with the formulation: $Bi_{2-2x}Cd_xPb_xO_{3-2x}F_{2x}$. For the composition $x=0.3$ ($Bi_{1.4}Cd_{0.3}Pb_{0.3}O_{2.4}F_{0.6}$), the spectrum is constituted of several well-defined narrow peaks, characteristic of a crystallized phase. In contrast, the spectra corresponding

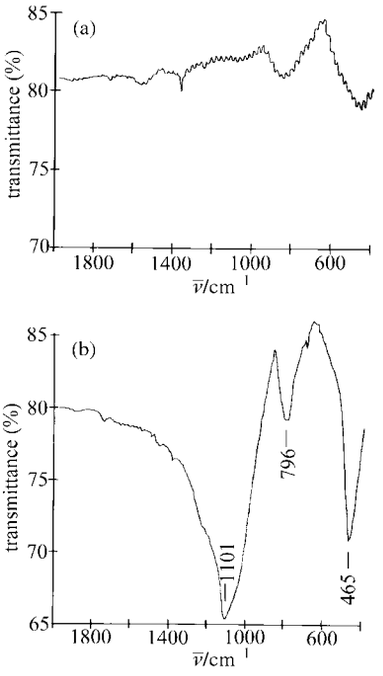

Fig. 4 IR spectra for (a) $Bi_{0.8}Cd_{0.6}Pb_{0.6}O_{1.8}F_{1.2}$ and (b) a silica tube.

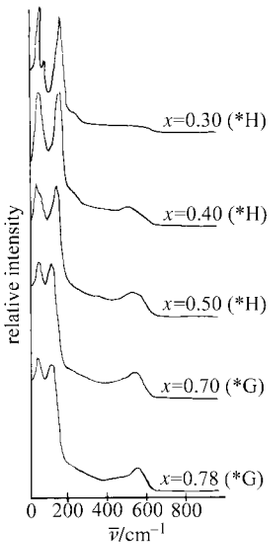

Fig. 5 Raman diffusion spectra for samples synthesized in gold tubes (* nature of the phase revealed by X-ray diffraction).

to $x=0.7$ ($Bi_{0.6}Cd_{0.7}Pb_{0.7}O_{1.6}F_{1.4}$) and $x=0.78$ ($Bi_{0.44}Cd_{0.78}Pb_{0.78}O_{1.44}F_{1.56}$) samples show the presence of a vitreous phase: this is illustrated by the presence of a wide double-band close, to $\bar{\nu}=200\ cm^{-1}$. This feature, which corresponds to boson peaks, has already been observed for lead glasses and is characteristic of this type of glass.[7] For the last two compositions $x=0.4$ ($Bi_{1.2}Cd_{0.4}Pb_{0.4}O_{2.2}F_{0.8}$) and $x=0.5$ ($Bi_1Cd_{0.5}Pb_{0.5}O_2F_1$), the Raman spectra exhibit an intermediate profile which reveals the coexistence of a vitreous phase and a crystalline one. This emphasizes the great sensitivity of Raman scattering as a tool to detect the presence of any intergranular vitreous phase along with a crystallized one. The existence of a glass had not been previously evidenced from DTA, lattice parameter evolution or conductivity measurements.

The Raman experiments performed on samples synthesized in silica tubes show that for the four studied compositions, the spectra (Fig. 6) are very similar and are characterized by a wide band with two peaks at $\bar{\nu}<200\ cm^{-1}$ and a very weak band at $600\ cm^{-1}$. This is in agreement with the existence of a vitreous phase.

The diffusion Raman study has shown that the H phase obtained in gold tubes is partly crystallized. This may be related to the different quenching conditions for gold tubes (slow quenching rates) and silica tubes (faster quenching rates). A similar experimental process is difficult to replicate with gold tubes because of their fragility in an oxyacetylene flame.

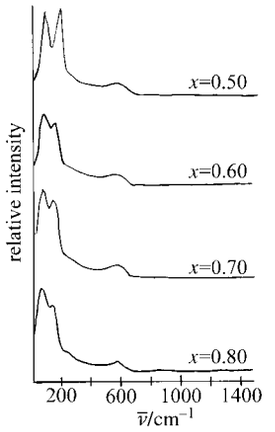

Fig. 6 Raman diffusion spectra for samples synthesized in silica tubes.

Conductivity measurements

Owing to the Raman results, we decided to measure the conductivity of samples synthesized in silica tubes and belonging to G′, which presents the largest glass composition domain. Measurements were performed on blocks heated at temperatures just below T_g, for one week. Compacities are greater than 88%.

Evolution of $\log\sigma$ with temperature for $Bi_{0.4}Cd_{0.56}Pb_{1.04}O_{1.16}F_{2.08}$. Fig. 7 shows the σ Arrhenius plot for a sample of composition $Bi_{0.4}Cd_{0.56}Pb_{1.04}O_{1.16}F_{2.08}$ (pseudo-binary c, with $x=0.8$), which is representative of the behavior over the whole domain. Several successive heating and cooling cycles were performed up to different maximum temperatures.

The conductivity curve shape is typical of a glass.[8] From 140 up to 200 °C (part I), $\log\sigma$ increases linearly with an activation energy of 0.54 eV. In this part, the glass phase exhibits the same behavior as a crystallized phase. As long as the highest temperature remains below T_g, all the heating and cooling cycles are reproducible.

When the measurement temperature becomes higher than T_g (part II), the conductivity no longer varies linearly. A new mechanism occurs which follows the law $\sigma=\sigma'_0\,e^{-\Delta E'/k(T-T_0)}$ with $T_0\cong 3/4T_g$.[8] In this domain, the glass behaves as a liquid and, owing to the network plasticity, the ion migration is enhanced.

In the third part of the curve, the temperature is now higher than T_c and crystallization of the material progressively occurs. Part IV of the curve corresponds to the conductivity of a fully crystallized phase. For the same temperature, σ is smaller for the crystallized phase than for the initial vitreous phase. Two activation energies are systematically observed: 0.73 eV at low temperature (below 260 °C) and 0.96 eV at high temperature for the present sample. This is in agreement with previous observations on oxyfluorides.[3] The origin of these two activation energy values has been attributed to the additional contribution of intrinsic defaults at high temperature.

For all the studied compositions, the conductivity curves are nearly identical. So, for glasses, only the curves below T_g were considered further.

Conductivity variation with composition. Fig. 8 and 9 respectively represent the variation of $\log\sigma$ *versus* the inverse temperature for vitreous and recrystallized samples belonging to the line Bi_2Cd_3–$PbCdOF_2$ (pseudo-binary a), with composition corresponding to $Bi_{2-2x}Pb_xCd_xO_{3-2x}F_{2x}$. This line was chosen because it is located in the largest glass domain.

For the two types of samples, σ increases with x (*i.e.* with

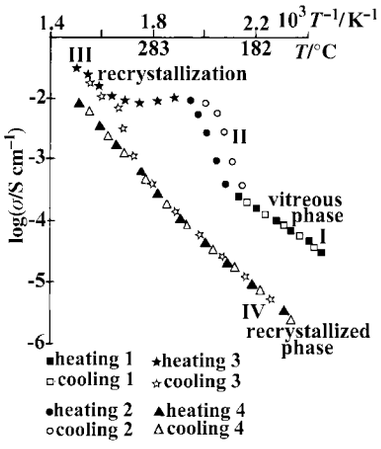

Fig. 7 Evolution of $\log\sigma$ with temperature for $Bi_{0.4}Pb_{0.56}Cd_{1.04}O_{1.16}F_{2.08}$.

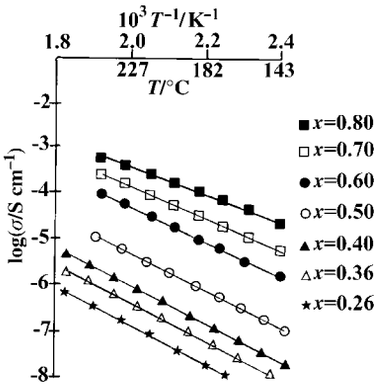

Fig. 8 Evolution of log σ with temperature for glasses belonging to the line Bi_2O_3–$PbCdOF_2$ ($Bi_{2-2x}Pb_xCd_xO_{3-2x}F_{2x}$).

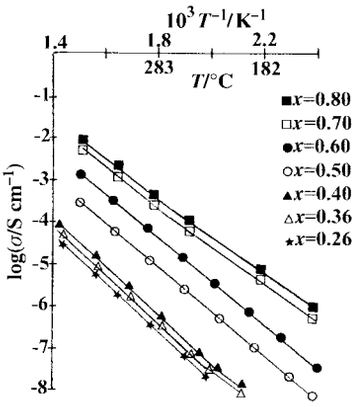

Fig. 9 Evolution of log σ with temperature for recrystallized samples.

fluorine ratio). This is well illustrated in Fig. 10 which represents the isothermal conductivity at 150 °C.

The best conductivity value is obtained for the composition $Bi_{0.4}Cd_{0.8}Pb_{0.6}O_{1.4}F_{1.6}$ ($\sigma = 1.5 \times 10^{-5}$ S cm^{-1}). Along the line, σ increases with the fluorine ratio and decreases with the oxygen ratio. This indicates that F^- ions are the main charge carriers. σ is close to values obtained for glasses belonging to the Bi_2O_3–PbO–CdF_2 system, which was recently studied[1] ($\sigma = 3 \times 10^{-5}$ S cm^{-1} at 150 °C). This figure also shows that the recrystallized phase conductivities are about one order of magnitude smaller than the glass conductivities.

Structural study of the recrystallized phase (H type)

Because we were unable to obtain crystals, the structure of the recrystallized phase was investigated by X-ray powder diffraction using a Siemens D5000 diffractometer in Bragg–Brentano geometry (θ, 2θ) and back-monochromated Cu-K_α radiation. The diffraction pattern was scanned in steps of 0.02° (2θ) over

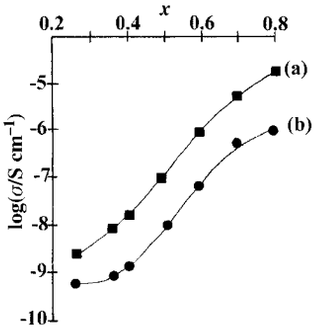

Fig. 10 Evolution at 150 °C of isothermal conductivity for glassy (a) and recrystallized (b) samples with x.

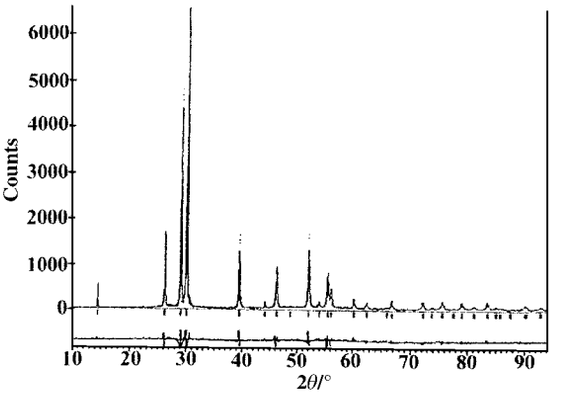

Fig. 11 Observed and experimental patterns for $Bi_{1.2}Cd_{0.4}Pb_{0.4}O_{2.2}F_{0.8}$.

the range 10–110°. The precise positions of the peaks were determined by means of the fitting program FIT, available in the PC software package DIFFRAC.AT from SOCABIM. Taking into account the similarity between the H phase of the Bi_2O_3–PbO–PbF_2 diagram and the recrystallized phase, the results obtained for the H phase are introduced as the basis of this resolution. Detailed structural work on the H phase belonging to the Bi_2O_3–PbO–PbF_2 diagram has been carried out by Follet-Houttemane and coworkers[3,9,10] on several compositions by X-ray diffraction and neutron diffraction. The main results may be summarized as follows: for all the samples, the cations are located in the 2d site of the $P\bar{3}m1$ space group ($Z = 1$). The anions are distributed over the 6i site, the 2c site, the 6h site and the 6g or 1a site. Evidently, it is not possible to distinguish oxide or fluorine ions, but the 6i site has been attributed to oxide ions, taking into account the cation–anion distance. Effectively, for the other anionic sites, the anion–cation distances are relatively high. This phenomenon could be due to the fluorine mobility which increases the cation–F^- distances. It is noted that the fluorine ions in the F(1) site occupy the 6g position, or the 1a position, according to the thermal treatment of the sample.

The crystal structure of $Bi_{1.2}Cd_{0.4}Pb_{0.4}O_{2.2}F_{0.8}$ (pseudo-binary a, $x = 0.4$) was refined by the Rietveld method,[11,12] on the basis of results found for $BiPbO_2F$[10] in the $P\bar{3}m1$ space group ($Z = 1$). The cell parameters were refined to $a = 3.9315(3)$ and $c = 6.164(3)$ Å. The cations are statistically distributed over the 2d site. Two oxide ions are placed in a 6i site, the remaining 0.2 oxide ions share a 2c site with 0.4 fluoride ions. Placing the remaining fluorine in the 6g site leads to an x value equal to 0, as for the 1a site. Table 2 summarizes the coordinates and the isotropic temperature factors for each crystallographic position.

At the end of the refinement process, the agreement between the observed and calculated data was indicated by the reliability factors:

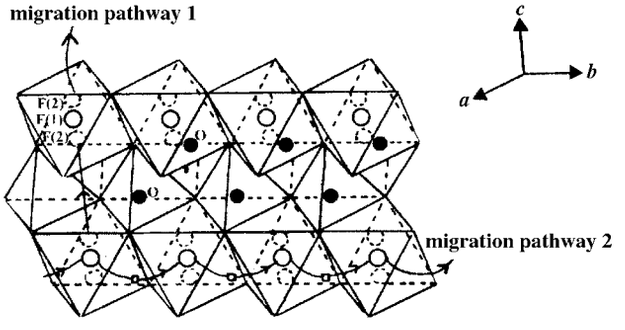

Fig. 12 Octahedral and pyramidal environments of F^- ions and tetrahedral environments of O^{2-} chains, plus a view of the migration pathways.

Table 2 Atomic coordinates and isotropic temperature factors of Bi^{3+}, Cd^{2+}, Pb^{2+}, O^{2-} and F^- for $Bi_{1.2}Cd_{0.4}Pb_{0.4}O_{2.2}F_{0.8}$

Atom	Ions number/site	Site	x	y	z	B/Å^2
Bi, Cd, Pb	2	2d	1/3	2/3	0.2637(3)	3.32(7)
O	2	6i	0.310(2)	0.620(2)	0.641(3)	3.3
F(1)	0.4	1a	0	0	0	4
F(2) (0.4 F^- + 0.2 O^{2-})	0.6	2c	0	0	0.1361(3)	3

$$R_{\text{Bragg}} = \Sigma_k |I_k - I_k^{\text{calc}}| / \Sigma_k I_k = 9.29\%$$

and

$$R_F = \Sigma ||F_{\text{obs}}| - |F_{\text{cal}}|| / \Sigma |F_{\text{obs}}| = 12.9\%$$

and by the representation of the observed and calculated patterns for $10^\circ < 2\theta < 120^\circ$ (Fig. 11).

The refinement converged at $\chi^2 = (R_{\text{wp}}/R_{\text{p}})^2 = 3.11$ for 60 reflections, with R_{wp} equal to 15.9 and R_{p} equal to 9.01.

The reliability factors have no best values, because of the small number of reflections.

The structure can be described as a hexagonal cation packing in which the anions partially occupy the vacancies of the cation network (Fig. 12). The anion environments are similar to those found for $BiPbO_2F$.[10] O^{2-} ions are distributed in tetrahedral sites denoted O and in pyramidal sites F(2). F^- ions are located in octahedral F(1) sites and in F(2) sites along the z axis. For the composition $Bi_{1.2}Cd_{0.4}Pb_{0.4}O_{2.2}F_{0.8}$, the only pathway available for anion migration is located in the c direction. No migration can occur in the perpendicular direction (xy plane) because the distance, d_1, between an empty tetrahedron and the neighboring oxygen sites is too small ($d_1 \approx 1.5$ Å).

This structural study confirms the analogy with the trigonal phase belonging to the Bi_2O_3–PbO–PbF_2 diagram;[3,9,10] *i.e.* when a sample contains an oxygen number per cell larger than 2, this oxygen excess is located in the fluorine pathway along the c axis and contributes to the anionic migration along this axis.

Conclusion

The study of the Bi_2O_3–CdO–PbF_2 phases system prepared by melting in silica tubes has shown the existence of a large vitreous domain.

Conductivity measurements lead to σ values of about 10^{-3} S cm^{-1} at 250 °C with an activation energy of 0.6 eV. These values are close to those obtained for $Pb_{0.75}Si_{0.25}O_{1.1}F_{0.30}$[13] and are larger than the σ values reported for $PbO_{0.3}F_{1.4}$.[13]

The recrystallized phase exhibits smaller conductivity values (one order of magnitude lower). Its structure is similar to that of the crystallized phase belonging to the Bi_2O_3–PbO–PbF_2 system.[9] Two types of anion pathways can be considered: the first along the z axis, and the second in the (xy) plane, which is only available for phases with an oxygen ratio lower than two.

Acknowledgements

We thank Dr. Annick Lorriaux-Rubens, from LASIR (Université Lille I C5, 59655 Villeneuve d'Ascq, France) for the Raman scattering experiments.

References

1 F. Désanglois and C. Follet-Houttemane, *Ann. Chim. Sci.*, 1998, **23**, 347.
2 S. F. Matar, Thèse d'Etat Bordeaux, 1983.
3 C. Follet-Houttemane, J. Canonne, J. C. Boivin, J. C. Champarnaud-Mesjard, D. Mercurio and B. Frit, *Solid State Ionics*, 1993, **66**, 267.
4 C. Follet-Houttemane, J. C. Boivin, J. C. Champarnaud-Mesjard, A. Aftati and B. Frit, *Solid State Ionics*, 1992, **57**, 265.
5 F. Désanglois, C. Follet-Houttemane and J. C. Boivin, *Solid State Ionics*, 1994, **70–71**, 229.
6 B. Govinda Rao, H. G. Keshava Sundar and K. J. Rao, *J. Chem. Soc., Faraday Trans 1*, 1984, **80**, 349.
7 S. Khatir, Thèse Lille, 1992.
8 C. Déportes, M. Duclot, P. Fabry, J. Fouletier, M. Hammou, M. Kleitz, E. Siebert and J. L. Souquet, *Electrochimie des Solides*, Editions Presses Universitaires de Grenoble, 1994.
9 C. Follet-Houttemane, J. Canonne, J. C. Boivin, J. C. Champarnaud-Mesjard, D. Mercurio and B. Frit, *Solid State Ionics*, 1988, **25**, 458.
10 J. C. Champarnaud-Mesjard, D. Mercurio, D. Frit, C. Follet-Houttemane, J. C. Boivin and G. Roult, *Eur. J. Solid State Inorg. Chem.*, 1989, **26**, 137.
11 H. M. Rietveld, *J. Appl. Crystallogr.*, 1967, **22**, 1151.
12 H. M. Rietveld, *J. Appl. Crystallogr.*, 1969, **2**, 65.
13 S. Goldammer, A. Runge and H. Kahnt, *Solid State Ionics*, 1994, **70–71**, 380.